

Application of Seismo-Acoustic Signals to the Study of Local Site Effects

Petru T. NEGRARU

Southern Methodist University, Department of Earth Sciences, Dallas, TX, USA
e-mail: pnegraru@smu.edu

Abstract

The Nevada Seismic Array (NVAR) is a small-aperture seismic array designed for monitoring an eventual nuclear test ban treaty. In spite of the 4 km aperture, large amplitude variations are recorded due to the complicated local geology. This study takes advantage of the collocated infrasound and seismic sensors to discuss the use of air-to-ground coupled waves to characterize the shallow geological structure existing beneath the array.

Complex transfer functions between the infrasound and the corresponding seismic signals are computed as the quotient of the cross-spectrum of the infrasound signal and the seismic signal and the power spectrum of the infrasound signal. Then the median of the transfer functions for the sites where shallow geologic information is available is compared to a theoretical model. In the theoretical approach, the signals are modeled as instantaneous pressure loads propagating at sound speed velocities (330 m/s). Both theory and observations are in agreement which suggests that inverting the transfer functions to determine elastic properties of the medium, and eventually computing site effects, is possible.

Key words: seismo-acoustic signals, infrasound area, seismic arrays.

1. INTRODUCTION

Ground motion peak acceleration maps are used by engineers to design earthquake resistant structures and to predict patterns of strong shaking from large earthquakes. The damage from the 1994 Northridge earthquake showed

irregular patterns across the Los Angeles area. Pockets of severely damaged buildings were located within 1 km of largely undamaged areas. This difference in damage was attributed to differences in the local site responses. Although the idea of high site amplification over short distances is widely accepted, a significant work on the topic has started only recently.

Extensive work has been done on quantifying the local site effects, with direct applications in engineering studies (seismic microzonation or prediction of earthquake strong motion). The common practice is to find site amplification factors based on the average shear wave velocity for the top 30 m of underlying materials (Borcherdt 1994, Boore and Joyner 1997). Engineering site investigations are usually limited to 30 m, and this has become a standard depth for classifying the site characteristics. Borcherdt (1994) and Martin and Dobry (1994) recommended that the design of structures be based on properties in the upper 30 m.

There are alternate methods to derive site amplifications which were widely studied and analyzed recently. The amplification factors are computed from coda waves (Mayeda *et al.* 1991, Phillips and Aki 1986, Su and Aki 1995) or from spectral ratio (Theodoulidis *et al.* 1996, Castro *et al.* 1997, Chen and Atkinson 2002, Siddiqi and Atkinson 2002), while comparisons among various techniques are discussed by Bonilla *et al.* (1997), Field and Jacob (1995), and Riepl *et al.* (1998).

The focus of this paper is on using seismic and infrasound signals to constrain near surface material properties. The first step is to detect the air-to-ground signals, and this will be performed by employing a detection algorithm based on the correlation coefficients between the infrasound and seismic sensors. From the signals thus detected, an empirical transfer function will be calculated and it will be matched with a theoretical pressure/velocity relationship.

2. DESCRIPTION OF THE NEVADA SEISMIC ARRAY SITE EFFECTS

A small-aperture array, the Nevada Seismic Array (NVAR), was installed in December 1998 by the Southern Methodist University (for details see NVAR Certification Manual 1999). The location of the array was chosen following the negotiations between a team of experts from the USA and Russia. It was decided that one of the three-component stations be located in the Black Butte mine, on the setting of the old MNV station for which historical records of nuclear explosions are available. Although the array fulfills its mission very well, to provide coverage for the Nevada Test Site (NTS) (Tibuleac and Herrin 2001), the final location, in a very complex tectonic and geological setting led to unusual site effects for a short-aperture array.

The array consists of ten short-period GS13 vertical seismometers with an aperture of 4 km (NV01 to NV10) disposed approximately in two circular alignments around a central station. An experimental infrasound array with the designation NVIAR (Nevada Infrasound Array) is collocated with the central short-period elements (NV01, NV02, NV03 and NV04). Three broadband three-component accelerometers (KS54000) are disposed around the array, forming an approximate equilateral triangle with the edge of 20 km (NV31 to NV33). With the exception of the NV31 and NV32, all the elements of the array are located in approximately 13.3 m deep boreholes. NV31 is located in the Black Butte mine, while NV32 is located in a deep borehole, at a depth of 60 m. The present study will focus mainly on the inner array (NV01 to NV04), which has collocated infrasound sensors.

The large amplitude variations at NVAR are evident without any kind of processing. Figure 1 shows the configuration of the short-period elements of the array and raw data from a 5.7 magnitude event that occurred in California. All the traces are at the same scale. By far the largest amplitude is recorded on channel NV04 (red trace), and in this particular case the variations reach factor three. These variations can be attributed to the shallow geology within the array. More than half of the stations are located in the Triassic limestone (sites NV01, NV02, NV03, NV05, NV06 and NV10). Sites NV04

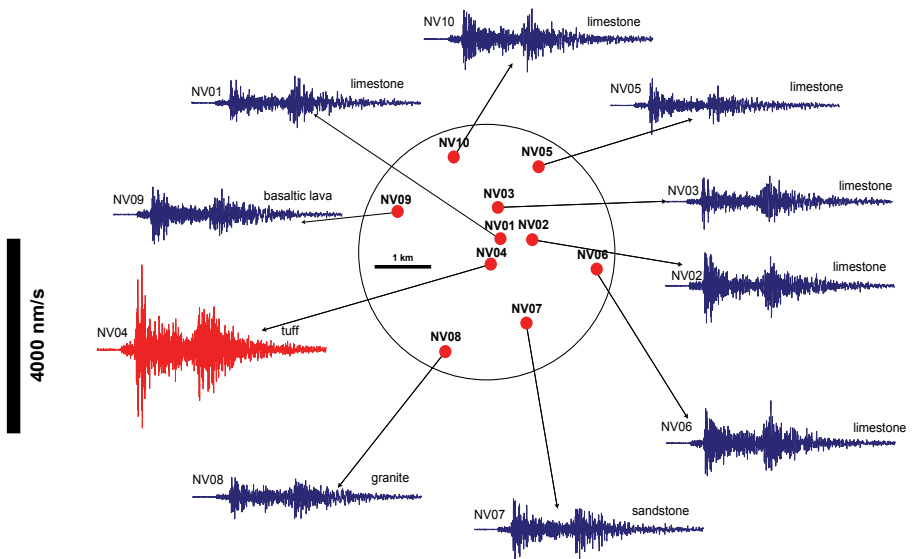


Fig. 1. Regional waveform recorded at NVAR, array configuration. Site NV32 is approximately 5 km south of site NV07. All the traces are shown at the same scale. The red trace is NV04 which shows the largest amplitude. In this case, the variations reach factor three. Colour version of this figure is available in electronic edition only.

and NV09 are located in volcanic rocks of Tertiary age (volcanic tuff, very variable in composition and texture and basaltic lava, respectively). Site NV07 is located in Jurassic sandstone (Dunlop Formation), while site NV08 is located in metamorphosed granite of Cretaceous age (for additional geological information see Stewart 1980).

Both NV04 and NV09 (located in younger geologic rocks) exhibit frequency dependent site amplifications, compared to any of the other sites of the array. At lower frequencies (up to 0.5 Hz), the signals are very similar and the amplitude variations are less than a factor of 2. However, above 1 Hz (up to 4 Hz) channel NV04 exhibits much larger amplitudes than the rest of the channels. In this frequency band, channels NV04 and NV01, only 500 m apart, have variations of up to a factor of 6. From 4 Hz to the antialias filter frequency (16 Hz), NV09 exhibits the largest amplitude, being sometimes more than one order of magnitude larger than the rest of the channels. No significant dependency on the source azimuth and distance has been found for these effects, which suggest the lack of any organized dipping structure beneath the array.

3. CHARACTERISTICS OF AIR-TO-GROUND COUPLED WAVES

Seismic detections of infrasound waves were reported several times (McDonald and Goforth 1969, Goforth and McDonald 1970, Sorrells *et al.* 1971a, b, 2002, Donn *et al.* 1971, Anglin and Haddon 1987, Langston 2004), even if sometimes no infrasound sensors were employed. It is uncommon to take advantage of the collocated infrasound and seismic arrays, though there are advantages in using seismic data in combination with infrasound, particularly in source characterization and discrimination at lower magnitudes, 2.5-4 m_b (Sorrells *et al.* 1997, Herrin *et al.* 1998, 1999, Chilo *et al.* 2006, Evers *et al.* 2007, Chilo 2008). In addition, for short-aperture seismic and infrasound arrays, the estimated azimuths of infrasound arrivals are thought to be more precise than the estimates based only on seismic arrivals, because the seismic wavefront can be highly distorted by the geologic structure. At the Texas Seismic Array (TXAR) located near Lajitas, Texas, the azimuths of seismic arrivals show differences up to $\pm 20^\circ$ in azimuth (Tibuleac and Herrin 1997), due to a dipping Moho beneath the array. In contrast, for the Columbia shuttle explosion which generated an infrasound signal, the estimated azimuths of the all the arrivals were all within $\pm 1.5^\circ$ (McKenna and Herrin 2006).

Early papers reported a correlation between changes in magnitude of the seismic and atmospheric pressure fields (Capon 1969a, b). Later it was determined that local fluctuations in the atmospheric pressure field can contribute significantly to the vertical seismic background noise, especially if the

seismic sensor is located in low-density, slow seismic velocity layers (Sorrells 1971).

McDonald and Goforth (1969) and Goforth and McDonald (1970) discuss the seismic effects of the sonic boom. In their study they employed collocated seismic and infrasound sensors. They found that the ground particle velocity is linearly related to the maximum pressure of the boom and to the geological properties of the ground. They also reported the presence of a precursor before the arrival of the maximum velocity which was always present when the velocity of the compressional wave in the ground was greater than the velocity of the aircraft (which gives the velocity of the N wave). Their interpretation suggested that the maximum particle velocity is associated with the passage of the N wave, and the smaller precursors are produced by air-coupled Rayleigh waves. Recently the air-coupled Rayleigh waves precursors were successfully modeled as “bow waves” originating at the advancing tip of the shock front trace (Sorrells *et al.* 2002).

A different approach was taken by Langston (2004) who computed synthetic seismograms to model the seismic ground motion caused by a bolide shock wave and concluded that the ground motions are generally confined to a near-surface layer of approximately 10 m, and they behave like high frequencies “leaky” and “locked” mode Rayleigh waves. He also suggested that the ground motions are not sensitive to the deeper earth structure, at least not in the Mississippi embayment.

4. DATA AND DATA PROCESSING

The seismo-acoustic signals (Fig. 2) were detected by estimating the correlation coefficients at zero lag between seismic and acoustic envelope functions for a sliding 10-second window. Because a shorter window yields higher correlation coefficients for seismic and infrasound noise, a tradeoff between window length and correlation threshold was achieved. The time length of most signals, which in general do not exceed a few seconds, was also taken into account. Empirically, a 10-second window and a detection threshold at 0.5 gave good results (Fig. 3). Typically the noise for such a window length has correlation coefficients that range from -0.3 to 0.3 while signals with good signal-to-noise ratio (SNR) have correlation coefficients above 0.5. The maximum correlation coefficient was 0.99, for a signal recorded on channel NV04. A detection was declared if there were correlation coefficients above 0.5 for at least three stations. With three stations, the backazimuth and the phase velocity can be computed. Although this method works well for NVAR, it is not expected to work in the same way for all stations in the western US, but a similar approach can be used to make a detector at each particular array (or site). Most of the signals detected at NVAR have

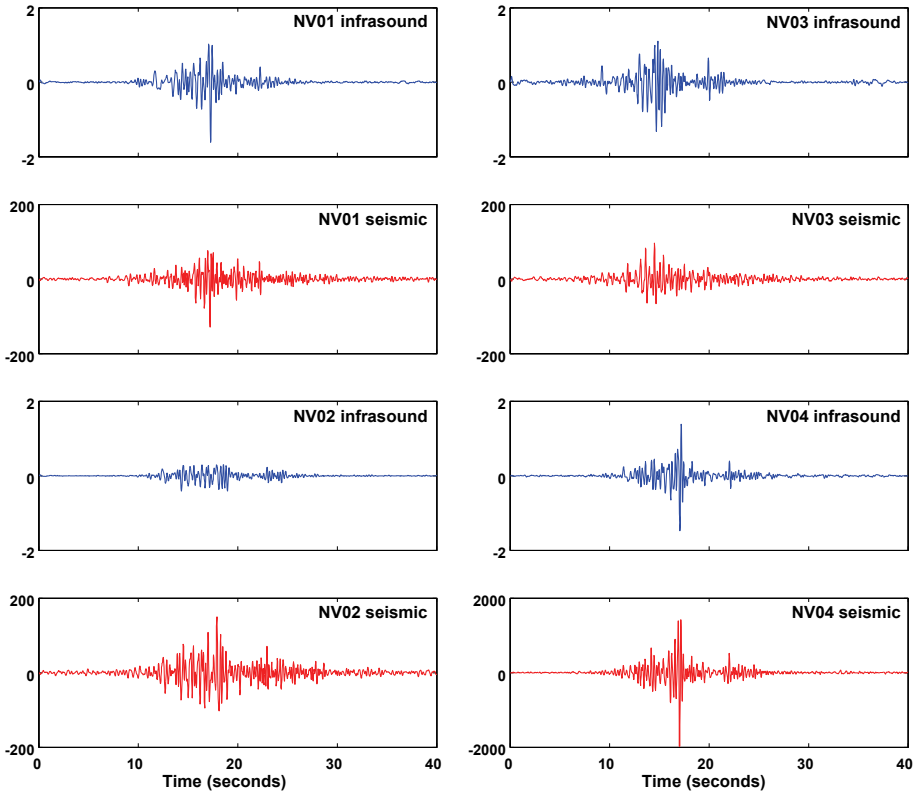


Fig. 2. Examples of air-to-ground coupled waves. The unit for seismic channels is nm/s, for infrasound is Pa. Shown here are the sites NV01 to NV04. Colour version of this figure is available in electronic edition only.

a dominant frequency around 2 Hz, well above the microbarom peak. Although a significant number of air-to-ground coupled signals were detected, due to low signal-to-noise ratio only 109 signals were selected for processing.

An important observation from Fig. 2 is that the infrasound arrivals exhibit significant phase and amplitude differences, in spite of the fact that the stations are only 500 m apart. Therefore, in the absence of infrasound sensors it is very difficult to extract quantitative information about the geologic structure. Infrasound signal decorrelation with distance is under investigation, but it appears that the infrasound signals are decorrelating faster than seismic signals.

For the signals detected and selected for processing, complex transfer functions were computed for the collocated infrasound and seismic channels. Transfer functions are the link between pressure signals and ground motions;

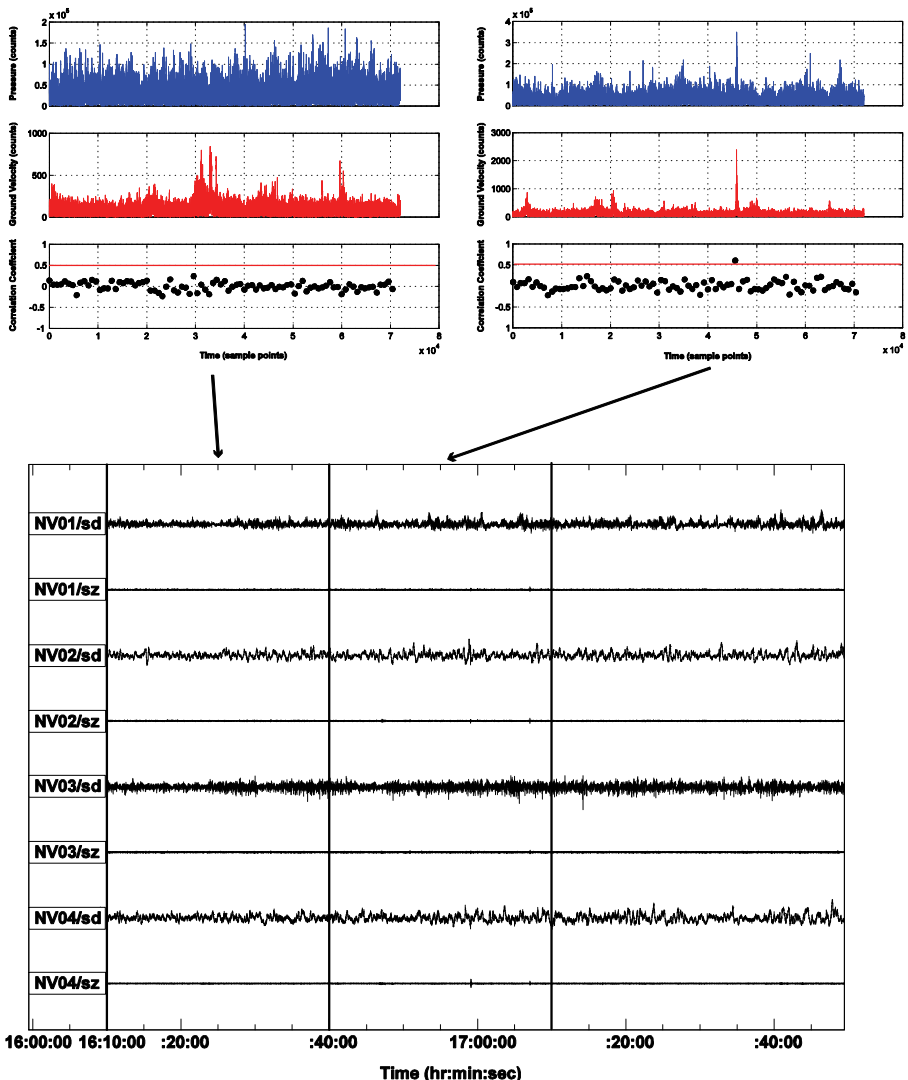


Fig. 3. Detection of seismo-acoustic signals. Colour version of this figure is available in electronic edition only.

they tell us how much ground motion is generated at a particular frequency for a given pressure signal. The whole air-to-ground coupling process could be regarded as filtering with a linear filter, where an input signal (the pressure signal) is filtered by the medium response to obtain an output signal (the seismic signal). What we need to find is the medium response (or the filter). The transfer functions were computed as the quotient of the cross-spectrum of the input signal (infrasound signal) and the output signal (seismic signal)

and the power spectrum of the input signal (infrasound signal). The approach makes use of Welch's averaged periodogram (Welch 1967) method. The length of each block was 64 points (1.6 seconds). The individual blocks in each sample record were overlapped by 50% and a Hanning window was used to reduce the variance of the estimate. Due to the short duration, the signals were also prewindowed using a Parzen window.

The magnitudes of the transfer functions have approximately similar shapes for the four channels (Fig. 4) with a certain amount of scatter for the

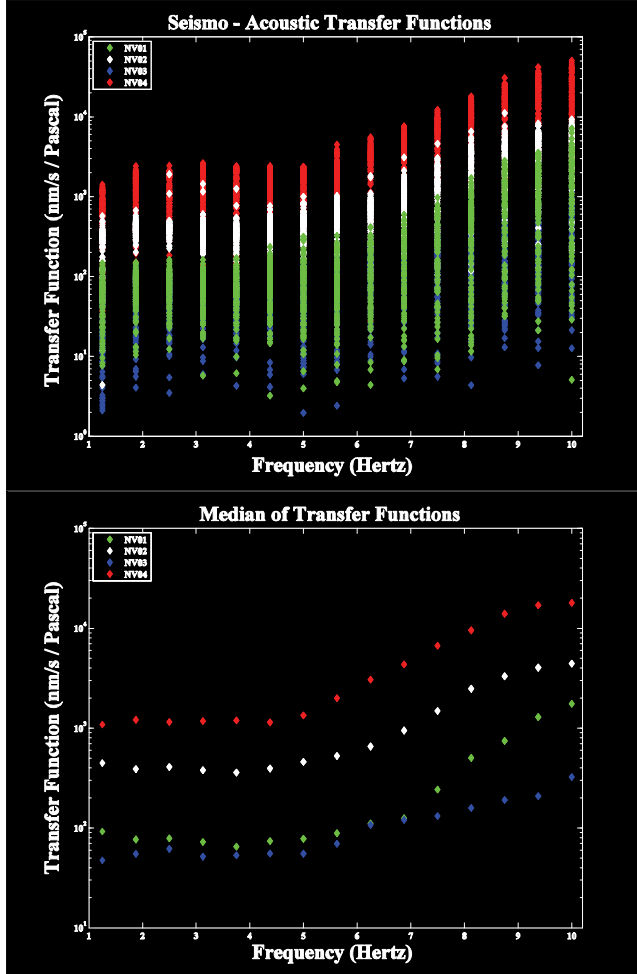


Fig. 4. Magnitudes of the transfer functions for the 109 signals selected for processing (upper plot), and the median of the transfer functions (lower plot). The increase above 5 Hz is due to P reverberations and P to S conversions in the very shallow layer. The approximately flat part of the spectrum up to 4 Hz is modeled as an atmospheric load. Colour version of this figure is available in electronic edition only.

low energy signals. The transfer functions are approximately flat to velocity/pressure up to 5 Hz, after which they start increasing. However, as expected, the magnitudes depend strongly on the site conditions. NV01 and NV03 are approximately at the same level, the median value for a 1 Pa pressure signal being 60 to 80 nm/s ground velocities for the flat part of the spectrum. At NV02, the ground velocities are more than 300 nm/s, while at NV04 the median ground velocities are on the order of 1200 nm/s, for the same 1 Pa pressure amplitude signal.

This increase above 5 Hz is represented by P reverberation and P to SV conversions in the shallow layers (approximately 10 m deep), with a mechanism similar to the one suggested by Langston (2004). However, in our case the short period vertical seismometers are located in approximately 13.3 m boreholes and coupled signals are recorded (though much attenuated) even by the broadband accelerometers located in competent granite at a depth of 60 m (station NV32). Therefore, the mechanism of coupling appears to be dominated by two effects: at low frequencies we model the amplitudes of the ground motion as instantaneous load, while at the high frequency the ground motions can be modeled with the approach suggested by Langston (2004). From a wavelength point of view, the lower frequency components of the signals have longer wavelength, and are insensitive to the finer structure, while the higher frequencies are sampling the shallower structure.

5. THEORETICAL ASPECTS

Sorrells (1971) was the first to derive an expression for the displacement ground response to a plane pressure wave, and a similar model slightly modified is adopted. The model is presented in detail in the Appendix, therefore only a brief discussion of it will be provided here.

The medium is approximated by a homogeneous and isotropic elastic half space. However, the velocity of the source wave (noted as c) is different. The original model (Sorrells 1971) was developed using wind speed velocities, much lower than the actual elastic velocities of the medium and the displacements were solved by approximation, finding the limit of the terms containing c^2 . In our case, the speed of the plane wave is the velocity of sound in air (around 330 m/s), much higher than the wind speed velocities, and even exceeding the shear wave velocity of the low-speed materials. Therefore, it is necessary to take into account all the terms. The final expression for the displacement response to a plane pressure wave is given in relations (9) and (10) from Appendix. These two relationships were used to compare the observed and the calculated velocities. It is also worth noting that in the previous studies the theory was compared with long period obser-

vations, generated by nuclear explosions, while in our case the signals are mostly high frequency, above 2 Hz.

The displacement relationships (eqs. 9 and 10 in Appendix) are depending on the material properties of the medium, have a $1/\omega$ dependency and a $\pi/2$ phase shift between the horizontal and vertical displacements, similarly to Rayleigh wave displacements. Beside the trivial solution there are 3 zeros, one for the vertical displacements and two for the horizontal displacements. The zero for the vertical velocities is reached when the velocity of the pressure waves equals the compressional speed velocity of the medium. This is actually the point where the polarizations of the induced waves change. All the infrasound signals used in this study have normal sound speed, below the compressional wave velocity of the medium. Therefore, the polarizations were not tested here, but changes in polarizations were observed for the ground motions induced by Arkansas bolide (Langston 2004). The other two zeros are reached for very high c values, $c = \pm\alpha^2/\sqrt{-\alpha^2 + 4\beta^2}$, which cannot be reached in a real physical model. Also note that when the velocity of the pressure wave exceeds the shear wave velocity of the medium, an additional phase shift is introduced.

6. DISCUSSION

To determine the physical properties of the medium necessary to compute the ground velocities, seismic refraction studies were conducted at sites NV01 and NV04 using a portable 12-channel EG&G seismograph and a BETSY seisgun seismic source. At NV01 the spacing of the geophones was 5 m, and the source was placed at 5 m offset. The medium increases gradually with depth in the upper 4 m from a very soft material (P -wave velocity of 457 m/s) to 2032 m/s at depth (Fig. 5). In addition, a shear geophone was lowered in the hole of the GS13 seismometer and an average velocity of 1520 m/s for the upper 12 m (the depth of the seismometer) was found. By weighting the velocities obtained through the seismic refraction survey with the layer thickness and then taking the average, an average value of 1507 m/s was obtained, close to the real result; therefore, the model appears to be accurate. The very soft nature of the upper layer could be observed on the first trace of the refraction profile, where the pressure wave arrives before the direct P wave.

A similar refraction survey at site NV04 (5 m spacing with 5 m offset) did not yield good results and the spacing of the geophones was increased to 10 m. The final model is composed of a layer over half space. The P -wave velocity of the upper layer is 570 m/s and has a thickness of approximately 30 m, and then the velocity increases to over 1800 m/s for the half space.

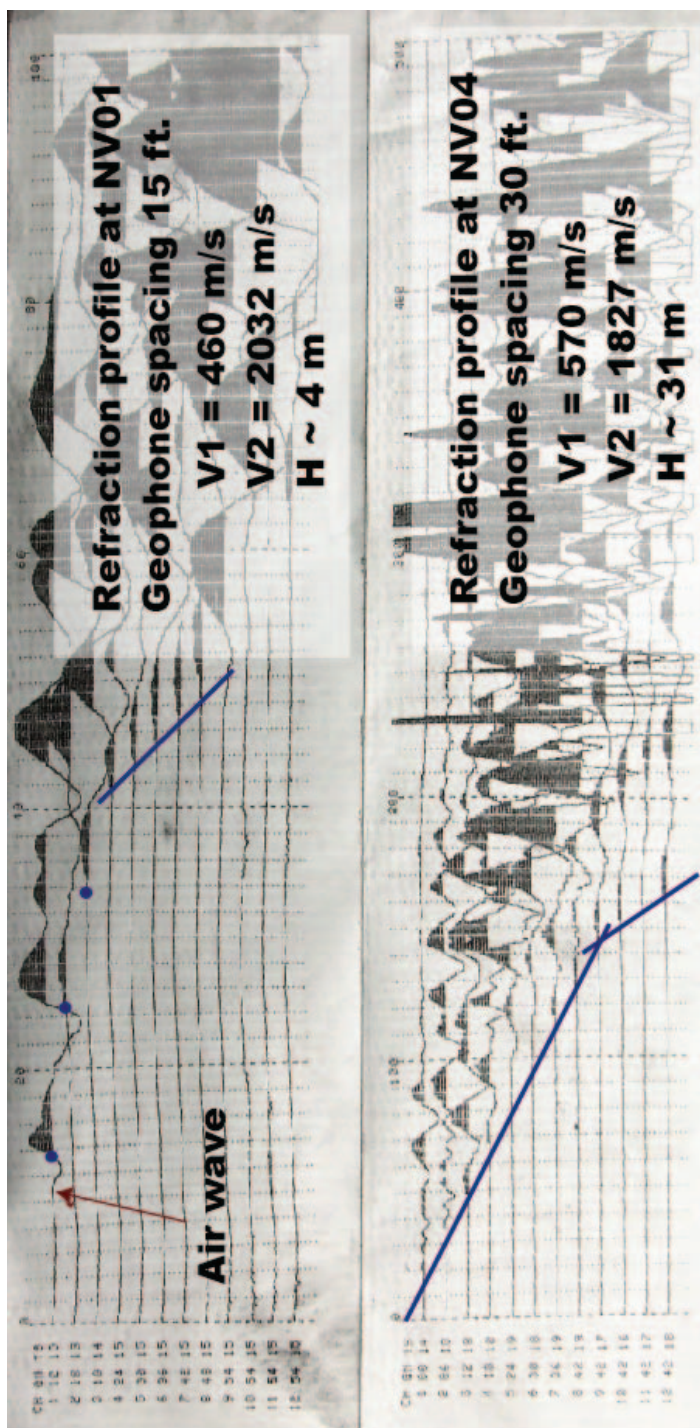


Fig. 5. Refraction profiles at NV01 and NV04 (photography of paper record).

The theoretical velocities were computed using relationships (9) (which includes the depth term, z) and (10) (which give the displacements at the surface) from Appendix multiplied with $i\omega$ to account for velocity and assuming values for the Poisson ratio necessary to compute shear velocities and elastic constants of the medium (Fig. 6). The shear wave velocity was computed assuming a 0.3 value for the Poisson ratio for both sites, and the density of the medium was assumed to be 2.75 g/cm^3 for NV01 (limestone) and 2.0 for NV04 (volcanic tuff). Good agreement with the observation was obtained for a P -wave velocity of 570 m/s for NV04 with no depth term and for 1975 m/s (close to the measured velocity), with a depth term of 12 m for NV01 (Fig. 6).

An interesting problem is how these signals attenuate with depth. The attenuation is frequency dependent, but it is also dependent on the medium properties (eqs. 9 from Appendix). The median of the transfer functions at NV01 shows a small decrease in the ground velocities from about 80 nm/s close 1 Hz to around 60 nm/s at 5 Hz. This decrease could be explained by introducing an attenuation term if we consider the depth of seismometer (approx. 12 m).

The attenuation with depth is best illustrated at site NV32 located in Garfield flats, in a homogeneous granite. Site NV32 is a KS54000 borehole accelerometer situated at a depth of 60 m. Because of the greater depth and

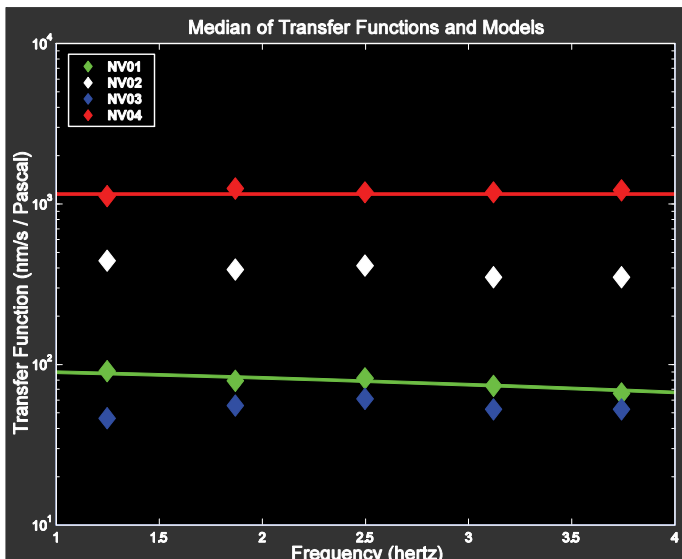


Fig. 6. Median of the transfer functions (filled diamonds) and computed velocities for sites NV01 and NV04 (solid lines). Colour version of this figure is available in electronic edition only.

the frequency content of signals, only a few of the large signals are observed on the seismometer. However, it is the only site which approaches the half space approximation. The Poisson ratio for such a medium is close to 2.5 and the P -wave velocity is at least 5800 m/s. Some infrasound signals with amplitudes of around 1 Pa on the infrasound sensors (amplitudes measured at NV01 to NV04) generated more than 20 nm/s² of ground motion on NV32. The computed ground accelerations were over 100 nm/s² at the surface for a 1 Pa amplitude pressure wave, while including an attenuation term the ground accelerations are 30 nm/s², which is well within the range of the observations. The most important disadvantage at this site is the lack of an infrasound sensor and there is no way of knowing whether the infrasound signal shown in Fig. 7 is weaker or stronger at site NV32, but even a weaker signal could not explain almost a factor of 4 in attenuation. Therefore, same decaying is due to the depths of the seismometer.

An application of these signals could be found by estimating site effects. An empirical approach would not work as the median spectral ratio

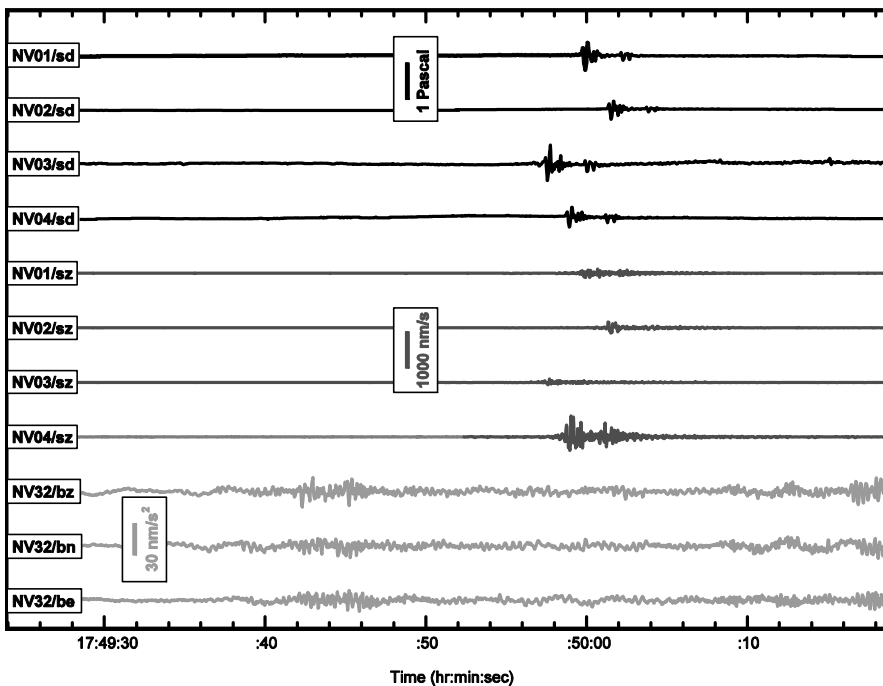


Fig. 7. Example of air-to-ground coupled waves at NV32. Site NV32 is located in granitic rocks at a depth of 60 m. The upper 4 traces (sd symbols) are the infrasound waveforms, the middle 4 traces (sz symbols) are the corresponding short-period waveforms, and the last three waveforms are observed vertical (bz) and horizontal (bn and be) ground motion components at site NV32.

NV04/NV01 of the purely seismic phases shows variations less than 4 in the 1-4 Hz frequency band, while the median ratio of the transfer functions shows variations more than one order of magnitude. In the standard approach proposed by USGS, site effects are estimated by using average shear wave velocity for the upper 30 m of the medium (Borcherdt 1994, Martin and Dobry 1994, and Boore and Joyner 1997). Therefore, accurate site effects could be obtained from air-to-ground coupled waves by inverting the transfer functions for average shear wave velocity (assuming values for the Poisson ratio) and then computing site effects. Both the observations and the theoretical approach suggest this is possible.

APPENDIX

In this Appendix we will derive an appropriate relationship for displacements in a isotropic and homogeneous half space due to a moving atmosphere load. The methodology is similar to the Sorrells (1971) approach, but certain modifications are required, and will be discussed in the text.

In a Cartesian coordinate system (x, y, z) we restrict movement only in x and z directions, therefore all the y components of the motion are null. Then the horizontal and vertical displacements can be written in terms of the potential functions $\Phi(\omega)$ and $\Psi(\omega)$ as

$$u = \frac{\partial \Phi}{\partial x} - \frac{\partial \Psi}{\partial z}, \quad w = \frac{\partial \Phi}{\partial z} + \frac{\partial \Psi}{\partial x}, \quad (1)$$

where the Heimholtz potentials can be written as

$$\begin{aligned} \Phi(\omega) &= A \exp \left[i(\omega t - kx) - z \sqrt{k^2 - \frac{\omega^2}{\alpha^2}} \right], \\ \Psi(\omega) &= B \exp \left[i(\omega t - kx) - z \sqrt{k^2 - \frac{\omega^2}{\alpha^2}} \right], \end{aligned} \quad (2)$$

where α is the compressional velocity of the half space, β is the shear velocity of the half space, ω is the angular frequency, A and B are constants to be determined from the initial conditions, and k is the wavenumber of the plane wave moving with the velocity c ($k = \omega/c$).

It can be shown that $\Phi(\omega)$ and $\Psi(\omega)$ satisfy the wave equation:

$$\begin{aligned}\nabla^2 \Phi &= \frac{1}{\alpha^2} \frac{\partial^2 \Phi}{\partial t^2}, \\ \nabla^2 \Psi &= \frac{1}{\beta^2} \frac{\partial^2 \Psi}{\partial t^2}.\end{aligned}\quad (3)$$

Then the vertical and horizontal stresses can be written as

$$\begin{aligned}p_z &= \lambda \nabla \Phi + 2\mu \left(\frac{\partial^2 \Phi}{\partial z^2} + \frac{\partial^2 \Psi}{\partial x \partial z} \right), \\ p_x &= \mu \left(2 \frac{\partial^2 \Phi}{\partial x \partial z} + \frac{\partial^2 \Psi}{\partial x^2} - \frac{\partial^2 \Psi}{\partial z^2} \right).\end{aligned}\quad (4)$$

A plane pressure wave moving with the velocity c can be written as

$$P(\omega) = P_0 \exp \left[i\omega \left(t - \frac{x}{c} \right) \right], \quad (5)$$

where P_0 is the amplitude of the pressure wave.

The initial conditions require that the horizontal stress vanish at the surface ($z = 0$) and the vertical stress is equal to the stress generated by the load. Therefore, from relations (4) and (5) we have:

$$\begin{aligned}p_z &= \lambda \nabla \Phi + 2\mu \left(\frac{\partial^2 \Phi}{\partial z^2} + \frac{\partial^2 \Psi}{\partial x \partial z} \right) = P(\omega), \\ p_x &= \mu \left(2 \frac{\partial^2 \Phi}{\partial x \partial z} + \frac{\partial^2 \Psi}{\partial x^2} - \frac{\partial^2 \Psi}{\partial z^2} \right) = 0.\end{aligned}\quad (6)$$

The resulting system has two unknown and two equations. Solving the system for A and B we obtain:

$$\begin{aligned}A &= \frac{P_0}{\frac{2\mu\omega^2}{c^2} - \frac{(\lambda+2\mu)\omega^2}{\alpha^2} + \frac{4\beta^2\mu\omega^2}{c^2-2\beta^2} \sqrt{\frac{1}{c^2} - \frac{1}{\alpha^2}} \sqrt{\frac{1}{c^2} - \frac{1}{\beta^2}}} , \\ B &= \frac{2ic^3P_0\alpha^2\beta^2}{\omega^2 \left[(c^2-2\beta^2) \left[-2\alpha^2\mu + c^2(\lambda+2\mu) \right] - 4c^2\alpha^2\beta^2\mu \sqrt{\frac{1}{c^2} - \frac{1}{\alpha^2}} \sqrt{\frac{1}{c^2} - \frac{1}{\beta^2}} \right]} .\end{aligned}\quad (7)$$

This result is replaced in eq. (2) and the potential functions can be written as

$$\Phi = \frac{c^2 P_0 \alpha^2 (c^2 - 2\beta^2) \exp \left[i(\omega t - kx) - z\omega \sqrt{\frac{1}{c^2} - \frac{1}{\alpha^2}} \right]}{\omega^2 \left[2\alpha^2 (c^2 - 2\beta^2) \mu - c^2 (c^2 - 2\beta^2) (\lambda + 2\mu) + 4c^2 \alpha^2 \beta^2 \mu \sqrt{\frac{1}{c^2} - \frac{1}{\alpha^2}} \sqrt{\frac{1}{c^2} - \frac{1}{\beta^2}} \right]}, \quad (8)$$

$$\Psi = \frac{2ic^3 P_0 \alpha^2 \beta^2 \sqrt{\frac{1}{c^2} - \frac{1}{\alpha^2}} \exp \left[i(\omega t - kx) - z\omega \sqrt{\frac{1}{c^2} - \frac{1}{\beta^2}} \right]}{\omega^2 \left[(c^2 - 2\beta^2) [-2\alpha^2 \mu + c^2 (\lambda + 2\mu)] - 4c^2 \alpha^2 \beta^2 \mu \sqrt{\frac{1}{c^2} - \frac{1}{\alpha^2}} \sqrt{\frac{1}{c^2} - \frac{1}{\beta^2}} \right]},$$

then the displacements can be computed from relation (1). The final form of the displacements is in eqs. (9) and (10):

$$u = \frac{ic P_0 \alpha^2 \left[\exp \left(z\omega \sqrt{\frac{1}{c^2} - \frac{1}{\beta^2}} \right) (c^2 - 2\beta^2) + 2c^2 \exp \left(z\omega \sqrt{\frac{1}{c^2} - \frac{1}{\alpha^2}} \right) \beta^2 \sqrt{\frac{1}{c^2} - \frac{1}{\alpha^2}} \sqrt{\frac{1}{c^2} - \frac{1}{\beta^2}} \right]}{\omega \left[(c^2 - 2\beta^2) [-2\alpha^2 \mu + c^2 (\lambda + 2\mu)] - 4c^2 \alpha^2 \beta^2 \mu \sqrt{\left(\frac{1}{c^2} - \frac{1}{\alpha^2} \right) \left(\frac{1}{c^2} - \frac{1}{\beta^2} \right)} \right]} \\ \times \exp \left[i(\omega t - kx) - z\omega \sqrt{\frac{1}{c^2} - \frac{1}{\alpha^2}} \sqrt{\frac{1}{c^2} - \frac{1}{\beta^2}} \right], \quad (9)$$

$$w = -\frac{c^2 P_0 \alpha^2 \sqrt{\frac{1}{c^2} - \frac{1}{\alpha^2}} \left[2 \exp \left(z\omega \sqrt{\frac{1}{c^2} - \frac{1}{\alpha^2}} \right) \beta^2 + \exp \left(z\omega \sqrt{\frac{1}{c^2} - \frac{1}{\beta^2}} \right) (c^2 - 2\beta^2) \right]}{\omega \left[2\alpha^2 \mu (c^2 - 2\beta^2) - c^2 (\lambda + 2\mu) (c^2 - 2\beta^2) + 4c^2 \alpha^2 \beta^2 \mu \sqrt{\frac{1}{c^2} - \frac{1}{\alpha^2}} \sqrt{\frac{1}{c^2} - \frac{1}{\beta^2}} \right]} \\ \times \exp \left[i(\omega t - kx) - z\omega \sqrt{\frac{1}{c^2} - \frac{1}{\alpha^2}} \sqrt{\frac{1}{c^2} - \frac{1}{\beta^2}} \right].$$

At the surface ($z = 0$) the displacements become:

$$u_0 = \frac{ic P_0 \alpha^2 \left[-2\beta^2 + c^2 + 2\beta^2 c^2 \sqrt{\frac{1}{c^2} - \frac{1}{\alpha^2}} \sqrt{\frac{1}{c^2} - \frac{1}{\beta^2}} \right] \exp [i(\omega t - kx)]}{\omega \left[(c^2 - 2\beta^2) [-2\alpha^2 \mu + c^2 (\lambda + 2\mu)] - 4c^2 \alpha^2 \beta^2 \mu \sqrt{\frac{1}{c^2} - \frac{1}{\alpha^2}} \sqrt{\frac{1}{c^2} - \frac{1}{\alpha^2}} \right]}, \quad (10)$$

$$w_0 = \frac{c^4 P_0 \alpha^2 \sqrt{\frac{1}{c^2} - \frac{1}{\alpha^2}} \exp [i(\omega t - kx)]}{\omega \left[2\alpha^2 \mu (c^2 - 2\beta^2) - c^2 (c^2 - 2\beta^2) (\lambda + 2\mu) + 4c^2 \alpha^2 \beta^2 \mu \sqrt{\frac{1}{c^2} - \frac{1}{\alpha^2}} \sqrt{\frac{1}{c^2} - \frac{1}{\beta^2}} \right]}.$$

In the original derivation of the formula (Sorrells 1971) velocity c is very small compared to the shear or compressional wave velocity of the medium and the expression was considerably simplified. In our case, the velocity is approximately constant and is equal to the velocity of sound in air ($c = 330$ m/s), and can even exceed the shear wave velocity of the medium for the soft materials. Therefore, all the terms need to be taken into account in the computation of the displacements. In addition, the observations used to match the theoretical displacements were long period recordings below 1 Hz, whereas the present study uses signals with dominant frequency around 2 Hz.

R e f e r e n c e s

- Anglin, F.M., and R.A.W. Haddon (1987), Meteoroid sonic shock-wave-generated seismic signals observed at a seismic array, *Nature* **328**, 607-609, DOI: 10.1038/328607a0.
- Bonilla, L.F., J.H. Steidl, G.T. Lindley, A.G. Tumarkin, and R.J. Archuleta (1997), Site amplification in the San Fernando Valley, California: Variability of site-effect estimation using the S-wave, coda and H/V methods, *Bull. Seism. Soc. Am.* **87**, 3, 710-730.
- Boore, D.M., and W.B. Joyner (1997), Site amplifications for generic rock sites, *Bull. Seism. Soc. Am.* **87**, 2, 327-341.
- Borcherdt, R.D. (1994), Estimates of site-dependent response spectra for design (methodology and justification), *Earthq. Spectra* **10**, 4, 617-653, DOI: 10.1193/1.1585791.
- Capon, J. (1969a), High-resolution frequency-wavenumber spectrum analysis, *Proc. IEEE* **57**, 8, 1408-1418, DOI: 10.1109/PROC.1969.7278.
- Capon, J. (1969b), Investigation of long-period noise at the Large Aperture Seismic Array, *J. Geophys. Res.* **74**, 12, 3182-3193, DOI: 10.1029/JB074i012p03182.
- Castro, R.R., M. Mucciarelli, F. Pacor, and C. Petrucciani (1997), S-wave site-response estimates using horizontal-to-vertical spectral ratios, *Bull. Seism. Soc. Am.* **87**, 1, 256-260.
- Chen, S.-Z., and G.M. Atkinson (2002), Global comparisons of earthquake source spectra, *Bull. Seism. Soc. Am.* **92**, 3, 885-895, DOI: 10.1785/0120010152.
- Chilo, J. (2008), Feature extraction for low-frequency signal classification, Ph.D. Thesis, Department of Physics, Royal Institute of Technology, Stockholm, Sweden.
- Chilo, J., A. Jabor, L. Liszka, Å.J. Eide, T. Lindblad, and L. Persson (2006), Infrasonic and seismic signals from earthquake and explosions in Arequipa, Peru, Western Pacific Geophysics Meeting, 24-27 July 2006, Beijing.

- Donn, W.L., I. Dalins, V. McCarty, M. Ewing, and G. Kaschak (1971), Air-coupled seismic waves at long range from Apollo launchings, *Geophys. J. Roy. Astron. Soc.* **26**, 1-4, 161-171, DOI: 10.1111/j.1365-246X.1971.tb03389.x.
- Evers, L.G., L. Ceranna, H.W. Haak, A. Le Pichon, and R.W. Whitaker (2007), A seismoacoustic analysis of the gas-pipeline explosion near Ghislenghien in Belgium, *Bull. Seism. Soc. Am.* **97**, 4147-425, DOI: 10.1785/0120060061.
- Field, E.H., and K.H. Jacob (1995), A comparison and test of various site-response estimation techniques, including three that are not reference-site dependent, *Bull. Seism. Soc. Am.* **85**, 4, 1127-1143.
- Goforth, T.T., and J.A. McDonald (1970), A physical interpretation of seismic waves induced by sonic booms, *J. Geophys. Res.* **75**, 26, 5087-5092, DOI: 10.1029/JB075i026p05087.
- Herrin, E.T., J. Bonner, P. Golden, C. Hayward, G. Sorrells, J. Swanson, and I.M. Tibuleac (1998), Reducing false alarms with seismo-acoustic synergy, Proc. 20th Annual Seismic Research Symposium on Monitoring a Comprehensive Nuclear-Test-Ban Treaty, 21-23 September 1998, Santa Fe, NM.
- Herrin, E., J.L. Bonner, P. Golden, C. Hayward, G.G. Sorrells, J. Swanson, and I.M. Tibuleac (1999), Reducing false alarms with seismo-acoustic synergy, Proc. 21st Seismic Research Symposium: Technologies for Monitoring the Comprehensive Nuclear-Test-Ban Treaty, 21-24 September 1999, Las Vegas, NV.
- Langston, C.A. (2004), Seismic ground motions from a bolide shock wave, *J. Geophys. Res.* **109**, B12309, DOI: 10.1029/2004JB003167.
- Martin, G.R., and R. Dobry (1994), Earthquake site response and seismic code provisions, *NCEER Bull.* **8**, 4, 1-6.
- Mayeda, K., S. Koyanagi, and K. Aki (1991), Site amplification from S-wave coda in the Long Valley caldera region, California, *Bull. Seism. Soc. Am.* **81**, 6, 2194-2213.
- McDonald, J.A., and T.T. Goforth (1969), Seismic effects of sonic booms: Empirical results, *J. Geophys. Res.* **74**, 10, 2637-2647, DOI: 10.1029/JB074i010p02637.
- McKenna, M.H., and E.T. Herrin (2006), Validation of infrasonic waveform modeling using observations of the STS107 failure upon reentry, *Geophys. Res. Lett.* **33**, L06811, DOI: 10.1029/2005GL024801.
- NVAR Certification Manual (1999), Prepared for the Preparatory Commission for the Comprehensive Nuclear-Test-Ban Treaty Organization Provisional Technical Secretariat International Monitoring System Division.
- Phillips, W.S., and K. Aki (1986), Site amplification of coda waves from local earthquakes in central California, *Bull. Seism. Soc. Am.* **76**, 3, 627-648.
- Riepl, J., P.-Y. Bard, D. Hatzfeld, C. Papaioannou, and S. Nechtschein (1998), Detailed evaluation of site-response estimation methods across and along the

- sedimentary valley of Volvi (EURO-SEISTEST), *Bull. Seism. Soc. Am.* **88**, 2, 448-502.
- Siddiqi, J., and G.M. Atkinson (2002), Ground-motion amplification at rock sites across Canada as determined from the horizontal-to-vertical component ratio, *Bull. Seism. Soc. Am.* **92**, 2, 877-884, DOI: 10.1785/0120010155.
- Sorrells, G.G. (1971), A preliminary investigation into the relationship between long-period seismic noise and local fluctuations in the atmospheric pressure field, *Geophys. J. Roy. Astron. Soc.* **26**, 1-4, 71-82, DOI: 10.1111/j.1365-246X.1971.tb03383.x.
- Sorrells, G.G., J.A. McDonald, Z.A. Der, and E.T. Herrin (1971a), Earth motion caused by local atmospheric pressure changes, *Geophys. J. Roy. Astron. Soc.* **26**, 1-4, 83-98, DOI: 10.1111/j.1365-246X.1971.tb03384.x.
- Sorrells, G., J.A. McDonald, and E.T. Herrin (1971b), Ground motions associated with acoustic waves, *Nature Physical Science* **229**, 14-16.
- Sorrells, G.G., E.T. Herrin, and J.L. Bonner (1997), Construction of regional ground truth databases using seismic and infrasound data, *Seismol. Res. Lett.* **68**, 743-752.
- Sorrells, G., J. Bonner, and E.T. Herrin (2002), Seismic precursors to space shuttle shock fronts, *Pure Appl. Geophys.* **159**, 5, 1153-1181, DOI: 10.1007/s00024-002-8676-0.
- Stewart, J.H. (1980), Geology of Nevada. A discussion to accompany the Geologic Map of Nevada, Nevada Bureau of Mines and Geology, Spec. Publ. 4, 136 pp.
- Su, F., and K. Aki (1995), Site amplification factors in Central and Southern California determined from coda waves, *Bull. Seism. Soc. Am.* **85**, 2, 452-466.
- Theodulidis, N., P.-Y. Bard, R. Archuleta, and M. Bouchon (1996), Horizontal-to-vertical spectral ratio and geological conditions: The case of Garner Valley Downhole Array in southern California, *Bull. Seism. Soc. Am.* **86**, 2, 306-319.
- Tibuleac, I.M., and E.T. Herrin (1997), Calibration studies at TXAR, *Seism. Res. Lett.* **68**, 353-365.
- Tibuleac, I.M., and E.T. Herrin (2001), Detection and location capability at NVAR for events on the Nevada test site, *Seism. Res. Lett.* **72**, 1, 97-107.
- Welch, P.D. (1967), The use of fast Fourier transform for the estimation of power spectra: A method based on time averaging over short modified periodograms, *IEEE Trans. AU* **15**, 70-73.

Received 12 June 2009

Received in revised form 31 March 2010

Accepted 8 April 2010